Structural and Electrochemical Study of Olivine Type LiFePO$_4$ as Cathode Material

A DISSERTATION REPORT

SUBMITTED IN PARTIAL FULFILMENT OF THE REQUIREMENTS FOR THE AWARD OF

THE DEGREE OF

MASTER OF SCIENCE

IN

PHYSICS

Submitted by:

Manish (2K21/MSCPHY/28)

Pinki (2K21/MSCPHY/37)

Under the Supervision of

DR. AMRISH K. PANWAR

DEPARTMENT OF APPLIED PHYSICS
DELHI TECHNOLOGICAL UNIVERSITY
(Formerly Delhi College of Engineering)
Bawana Road, Delhi -110042

CANDIDATE'S DECLARATION

We Manish (2K21/MSCPHY/28) and Pinki (2K21/MSCPHY/37) students of M.Sc. Physics, hereby certify that the work which is presented in the dissertation titled **"Structural and Electrochemical Study of Olivine Type LiFePO₄ as Cathode Material"** in fulfilment of the requirement for the award of Degree of Master of Science in Physics and submitted to the Department of Applied Physics. Delhi Technological University (Formerly Delhi College of Engineering), New Delhi is an authentic record of our own carried out during a period from January 2023 to May 2023, under the supervision of Dr. Amrish K. Panwar, Department of Applied Physics.

The matter presented in this report has not been submitted or previously formed the basis for the award of any Degree, Diploma, Associateship, Fellowship, or other similar title or recognition.
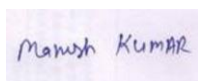
Title of Paper: *"Structural, morphological, electrical, and electrochemical performance of* $LiFePO_4$ *synthesized using ball milling"*

Authors names (in sequence as per research paper): Manish, Pinki, Amrish K. Panwar

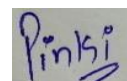**Conference:** International Conference on "Advanced Materials for Emerging Technologies" (ICAMET-2023)

Have you registered for conference(Yes/No)?: Yes

Conference Date: May 04-06, 2023

MANISH   PINKI

2K21/MSCPHY/28   2K21/MSCPHY/37

CERTIFICATE

I hereby certify that the Project Dissertation titled **"Structural and Electrochemical Study of Olivine Type LiFePO$_4$ as Cathode Material"** which is submitted by Manish (2K21/MSCPHY/28) and Pinki (2K21/MSCPHY/37) Department of Applied Physics, Delhi Technological University, New Delhi in partial fulfilment of the requirement for the award of the Degree of Master of Science is a record of the project work carried out by the students under my supervision and guidance.

To the best of my knowledge, this work has not been submitted in part or full for any Degree or Diploma to this University/Institute or elsewhere.

Date: 30th May 2023

Place: New Delhi

Dr. Amrish K. Panwar
Assistant Professor
Department of Applied Physics
Delhi Technological University

ACKNOWLEDGEMENT

ABSTRACT

This study is intended to synthesize the olivine-type pristine $LiFePO_4$ (LFP) using the solid-state ball milling method. The structural, electrical, and electrochemical properties of as synthesized pristine $LiFePO_4$ has been analyzed. The synthesized sample was characterized using X-ray diffraction (XRD) to confirm the single/mixed phase formation of the olivine type LFP as a cathode material. Hence, the Rietveld refinement analysis of the observed XRD pattern indicates that olivine type orthorhombic single phase with the space group, Pnma is formed without any impurity. Fourier Transform Infrared Spectroscopy (FTIR) is also performed to see the groups developed, bond strength and bond stretching and bond vibrations in the LFP. The dc conductivity and activation energy were estimated by the source measurement unit using Arrhenius equation. The electrochemical performance of LFP has been carried using Cyclic Voltammetry (CV), Electrochemical impedance spectroscopy (EIS) and Galvanostatic charge/discharge (GCD) methods. Here, it is found that the 1st cycle of pristine LFP delivers a specific discharge capacity of $52(\pm5)$ mAh g^{-1} at 0.5C rate and after 50 charge/discharge cycles a noticeable retention in the capacity is observed which implies that, the electrochemical Li^+ insertion/extraction process is extremely reversible and that the structure of pristine $LiFePO_4$ is quite stable and also the pristine LFP has a coulombic efficiency of greater than 99 %.

Keywords: Pristine LFP; Rietveld refinement; Olivine; Solid-state method.

CONTENTS

LIST OF FIGURES

LIST OF GRAPHS

LIST OF TABLES

CHAPTER 1
INTRODUCTION AND LITERATURE REVIEW

1.1 INTRODUCTION

Li-ion batteries, are a form of rechargeable battery that has become quite popular because of its real life integrating applications in different electronic products and electric cars. They are renowned for their substantial cycle life, high energy density, and relatively low self-discharge rate. Lithium-ion batteries have a high energy density compared to other rechargeable battery technologies, which allows them to store a lot of energy given their size and weight. They are therefore perfect for portable electronics like laptops, tablets, and cell-phones. Li-ion batteries can maintain their charge for a longer time when not in use because of their relatively low self-discharge rate. Lithium-ion batteries do have certain restrictions, though. They may be susceptible to thermal runaway and overheating if not carefully controlled since they may be sensitive to high temperatures. Although manufacturers adopt numerous safety systems to reduce these dangers, this can still raise safety concerns. Battery deterioration over time is a problem as well because a Li-ion battery's capacity gradually decreases [1].

1.2 HISTORY OF BATTERY

The founding father and polymath of the United States, Benjamin Franklin, introduced the term "Battery" to describe a network of connected capacitors in the 1749s when doing electrical experiments. The first really recognised battery names emerged later in the 1800s. Alessandro Volta created the voltaic pile, which consists of a layer of fabric acting as the electrolyte and a pair of zinc and copper discs that have been pilled on top of one another. The voltaic pile battery experienced issues like electrolyte leakage and short circuits [2].

1.3 TYPES OF BATTERIES

Batteries are classified mainly in two categories:

1.3.1 Primary Battery:

Primary batteries, commonly referred to as non-rechargeable or disposable batteries, are a category of battery that can only be used once and cannot be recharged. Primary batteries cannot be returned to their original state once the chemical reactions inside the battery have run their course; they must be replaced. The most common example of primary batteries is leclanche cell. Carbon is act as Cathode which is circumscribe by powdered carbon and manganese dioxide, and the cell is composed of a zinc field that continues to act as the anode (Fig.1). A wet paste made of ammonium chloride (NH_4Cl) and zinc chloride ($ZnCl_2$) comprises the space between the electrodes. Despite the complexity of the electrode reactions, the following may be said about them:

Anode: $Zn(s) \rightarrow Zn^{2+} + 2e\text{-}$ (1)

Cathode: $MnO_2 + NH_4^+ + e^- \rightarrow MnO(OH) + NH_3$ (2)

At cathode Manganese is reduces from the +4 to the +3 oxidation state. The reaction produces ammonia, which combines with zinc to give $[Zn\,(NH_3)_4]^{2+}$.
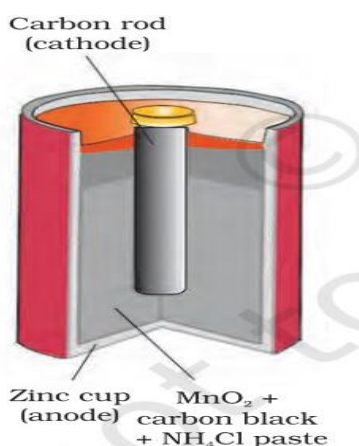
Fig 1.1: A commercial dry cell comprising graphite (carbon) as cathode and zinc container as anode

1.3.2 Secondary Battery:

 Secondary batteries are kind of rechargeable batteries that can be recharged by passing current through it after they are used completely. A spectacular secondary cell is capable of a variety of cycles of charging and discharging. Lead acid battery is the most efficient secondary battery, which is widely employed in motors and invertors. It contains a lead anode and a grid of lead loaded with lead dioxide (PbO_2). A 38% concentration of sulfuric acid in a solution is an electrolyte.

Below are the mobile reactions occurring at anode and cathode respectively in a lead acid battery :

Anode: $Pb(s) + SO_4^{2-}(aq) \rightarrow PbSO_4\ (s) + 2e^-$ $\qquad\qquad\qquad\qquad\qquad\qquad$ (3)

Cathode: $PbO_2\ (s) + SO_4^{2-}(aq) + 4H^+\ (aq) + 2e^- \rightarrow PbSO_4\ (s) + 2H_2O\ (I\ )$ $\qquad\qquad$ (4)
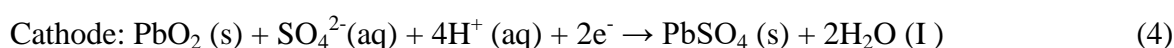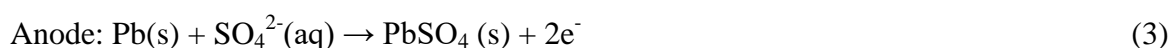
The overall reaction of a lead acid battery can be written as:

$Pb(s) + PbO_2\ (s) + 2H_2SO_4\ (aq) \rightarrow 2PbSO_4\ (s) + 2H_2O(I)$ $\qquad\qquad\qquad\qquad$ (5)
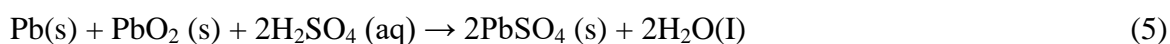
During charging $PbSO_4$ (s) transformed into Pb and PbO_2 at anode and cathode , respectively.

1.4 LITHIUM-ION BATTERIES

Lithium is one of the most useful materials in electrochemical research since it is the lightest metallic element in the periodic table, has the greatest electrochemical potential, and has the highest specific energy (Wh/Kg). Using a high energy thickness anode leads to dendrites formation which results in less cycle life. To overcome this issue the most widely used battery technologies at the moment is the lithium-ion battery. Energy and power density are the most crucial criterion to find which is fulfilled by lithium-ion battery. A few examples which includes lithium -ion batteries are electrical and hybrid automobiles as well as another crucial industry, energy storage systems.

1.5 WORKING PRINCIPLE OF BATTERY

The three crucial components of a rechargeable battery or cell are depicted in Fig.2 as the cathode (the positive electrode), anode (the negative electrode), and electrolyte which are separated by a membrane called separator. The degree of attraction or affinity for the electrons exhibited by various types of metals and their compounds varies. The ions can flow between the anode and cathode during charge and discharge cycles through the electrolyte, a conductive liquid. Ions are transported from the cathode to the anode during charging and are then stored in the anode structure by travelling through the electrolyte. The battery can be recharged because this process is reversible. The lithium ions return to the cathode once the battery is depleted, releasing energy in the form of electrical current.
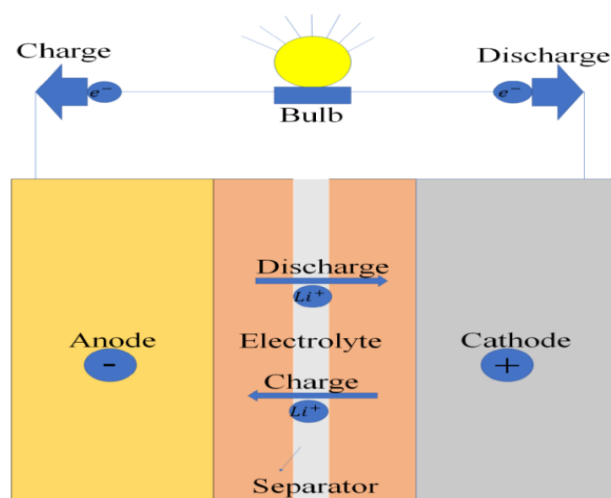
Figure 1.2: Schematic diagram of a Li-ion battery with liquid electrolyte.

Let's take an example of typical $LiCoO_2$ cathode and graphite anode based lithium-ion battery. When an external electric current is applied, then during charging of cell, lithium-ion move out of the cathode ($Li_{1-x}CoO_2$) passing through electrolyte and separator and then intercalated inside the anode (Li_xC_6) converting electrical energy into chemical energy. In contrast, as the cell is being discharged, lithium ions return to the cathode and release the

chemical energy that had been stored by creating an external electrical current. Hence, the electrochemical reactions in these kind of cells are as follows [3], [4]:

$$Li_{1-x}CoO_2 + xLi^+ + xe^- \leftrightarrow LiCoO_2 \tag{6}$$

$$Li_xC \leftrightarrow C + xLi^+ + xe^- \tag{7}$$

$$Li_xC + Li_{1-x}CoO_2 \leftrightarrow C + LiCoO_2 \tag{8}$$

1.6 CATHODES

The intercalation and de-intercalation of Li-ions is the foundation of Li-ion batteries. Ions from the cathode are introduced into the anode's lattice structure during charging, and vice versa. The battery voltage is substantially impacted by the cathode material. The redox potentials of various cathode materials affect the voltage at which the battery runs. Cathode materials also impact the energy density in such a way that higher energy densities can store more energy per unit mass or volume, increasing the battery's overall capacity for energy storage. The cathode material also influences the battery's cycle life, power capacity, and safety, among other performance traits. These variables are influenced by the distinctive features of various cathode materials. For instance, compared to other cathode materials, lithium iron phosphate offers greater safety and a longer cycle life.

1.7 STRUCTURE OF CATHODES:

1) **Layered structure**

The layered structure adopts the general formula A_xMO_2 where A is alkali cation, M is metal cation and O is oxygen atom. In the oxygen framework's abc repeat unit, the A and M cations alternate to produce the stacking structure a-b_c-a_b-c, where the underscore "_" designates the position of the A ions and the minus sign "-" designates the location of the M ions. Periodicity is reached after six oxygen

layers since the oxygen stacking has a repeat unit of three and the metal layering repeats every two layers [4] [5]. Examples: $LiCoO_2$, $LiMnO_2$, $LiNiMnCoO_2$, $LiNiCoAlO_2$, Li_2MnO_3

2) Spinel Structure

The spinel structure is formulated as $MM_2`X_4$ where M and M` are tetrahedrally and octahedrally coordinated cations and X is anion. Spinal structure crystallize in cubic close-packed oxides with four octahedral and eight tetrahedral sites [6]. Examples: $LiMn_2O_4$, $LiCo_2O_4$

3) Olivine structure

The Olivine structure is formulated as ABC_4 where A and B are tetrahedrally and octahedrally coordinated cations and C is anion Olivine crystallize in orthorhombic system (space group Pbnm). The structure can be described as HCP array of oxygen ions with half of octahedral sites occupied with Mn or Fe or Co ions and 1/8 of tetrahedral sites occupied by silicon ions [7]. Examples: $LiFePO_4$, $LiMnPO_4$, $LiCoPO_4$.

4) Tavorite Structure

Tavorite Structure consist of Triclinic and 2-D orthorhombic (Pbcn space group) and tunnel like monoclinic (P 21/n space group) [8]. Examples: $LiFeSO_4F$, $LiVPO_4F$

1.8 LITHIUM IRON PHOSPHATE (LiFePO$_4$)

Lithium Iron Phosphate (LFP) is a cathode material used in Lithium -ion batteries. The nominal voltage of LFP is 3.2 V [9], [10] . In recent years it has drawn a lot of interest due to its special properties and benefits in many real life applications which includes Energy storage devices, Backup power system, Electric vehicles, Renewable energy system and many more. $LiFePO_4$ has several advantages, including:

1. Safer to use and less prone to thermal runaway.

2. Excellent cycle life.

3. High Power capability.

4. Environment friendly.

5. Non-toxic.

6. Low cost.

1.8 LITERATURE REVIEW

B.M. Kerbela, L.M. Katsnelsonb, Yu.V. Falkovichc [11], looked into the air-based synthesis of carbon-coated lithium iron phosphate. Without creating an oxygen-free medium, $LiFePO_4$/C was synthesised using the solid state technique in a furnace reaction chamber using a naturally inert medium. The conditions for reducing medium to form in the synthesis zone directly from gaseous synthesis products were established. Following factors were identified as the best ones for LFP synthesis using the solid state method: A) synthesis temperature of less than 850 °C; B) a synthesis time of one minute; and; C) wet mixing of the precursors with hot distilled water in a ball mill for 24 hours. Under ideal circumstances, the specific discharge capacity was 136.4 mAh/g (converted to the weight content of the active material), and after 20 cycles, there was no appreciable capacity degradation. Dispersive crystal nanocomposites made of porous granules having a network of linked

channels are known as LiFePO$_4$/C powders. This distinct structure increases the potential for usage as a cathode material in electrochemical processes and improves the yield of lithium ions in the electrolyte.

Yingtang Zhang, Pengyang Xin, Qiufeng Yao [12]**,** see the electrochemical performance of LiFePO$_4$/C synthesised using the sol-gel method, and made every effort made to address issues with poor cycling stability and low energy density by regulating the quantity and LiFePO$_4$ particles are dispersed uniformly, and carbon is coated to increase their electronic conductivity. Homogenous conductive carbon's beneficial effects, which guarantee the bulk electrode's continuous electrical contact and nanoscale Li-ion diffusion channel, may be responsible for the better electrochemical performance. In comparison to LiFePO$_4$, LiFePO$_4$/C shows stronger polarisation between the anodic and cathodic peaks and more reversible ion insertion/extraction. The LiFePO$_4$/C exhibits an excellent capacity retention of 8.9% after 110 cycles and a high reversible capacity of 163.5 mAh/g at a current rate of 0.1C. The findings show that the rate capability and cycle stability of the LiFePO$_4$ material are significantly influenced by the surface shape and homogeneous conductive carbon .

C.H. Mi a, Y.X. Cao, X.G. Zhang, X.B. Zhao, H.L. Li [13] studied new class of composite cathodes made of nanoscale carbon webs that were made using the aqueous co-precipitation and sol-gel processes, respectively. The olivine structure of LiFePO$_4$ is unaffected by the silver and carbon co-modifying, but its dynamics have been improved in terms of discharge capacity and rate capability. Using the co-precipitation and sol-gel methods, LiFePO$_4$/(Ag+C) cathodes' discharge capabilities increased from 153.4 mAh/g of LiFePO$_4$/C to 160.5 mAh/g and 162.1 mAh/g, respectively. The charge transfer resistance of LiFePO$_4$/(Ag+C) cathodes is shown to be reduced by the co-modification of Ag + C by AC impedance measurements.By doping with guest cations or by covering the LiFePO$_4$ particle's electron conducting layer

with materials including carbon, copper, and silver. The second method is altering the synthesis conditions, such as utilising a wet-chemical technique or lowering the temperature during solid-state calcination, in order to reduce particle size. Additionally, it was discovered that co-modification of LiFePO$_4$ with carbon and silver might improve its surface electrical conductivity but not its bulk conductivity.

Rakesh Saroha , Amrish K. Panwar , Yogesh Sharma , Pawan K. Tyagi , Sudipto Ghosh [14] synthesized ZnO-doped LFP with the use of ball milling and sol gel. Higher ZnO concentrations don't cause bare LiFePO$_4$ to lose its structure. The addition of Zn to the LiFePO$_4$ lattice creates a sort of "pillar effect" that creates more room for the flow of lithium ions which ultimately increases the conductivity of LiFePO$_4$, as has its lithium ion diffusion coefficient. LFPZ2.5 has the best conductivity and largest discharge capacity of all the ZnO-doped samples thanks to its lowest AC resistance. Characterization data show that the quantity of ZnO is a key element in the enhancement of the lithium-ion. The upper layer of the cathode active material is coated with carbon to increase conductivity and electrochemical performance. The LFPZ2.5 sample had the highest redox intensity in the host lattice material, which indicates the fastest lithium ion migration and, as a result, higher electrode reaction reversibility. Due to high energy and power density LFP2.5 shows a prominent applications in EVs.

Rakesh Saroha and Amrish K. Panwar 2017 [15], investigate the physicochemical and electrochemical performance of bare LiFePO$_4$ (LFP) using ball milling route. The results of using acetylene gas as a carbon source and performing in-situ pyrolysis. Acetylene gas is employed as a carbon source for the surface coating of LFP particles since it decomposes into carbon and methane as well as various side products when exposed to high temperatures. In addition to improving electrical conductivity, carbon also regulates particle size by preventing

agglomeration. Whether the coating is crystalline or amorphous depends on the type of carbon source. Electrical conductivity tests reveal that the acetylene-treated LFP samples exhibit a conducting nature with a higher level of electronic conductivity than untreated LFP. According to electrochemical data, among all the synthesised samples, LFPC10 has the greatest specific discharge capacity and the best electrochemical characteristics. LFPC10 has high power density and excellent energy which makes its effective for use in automobile industry.

Jungbae Lee, Purushottam Kumar, Gwangwon Lee, Brij M. Moudgil & Rajiv K. Singh [16] , Examines the electrochemical performance of LFP produced by a solid-state reaction as a lithium-ion battery cathode material in comparison to unprocessed LFP and the impact of adding surfactant as a dispersion agent during high energy ball milling of precursor materials for LFP. When anionic surfactant was employed, LFP particles displayed improved size uniformity, morphological control, and decreased particle size. After adding surfactant during milling, the specific surface area of LFP particles rose by around a factor of two. Due to less polarisation of the electrode material, these particles demonstrated significantly improved cycle performance during charge/discharge. During the creation of the slurry, surfactants were utilised to scatter the electrode components. Author investigates the impact of surfactant addition on LFP particle size, shape, and electrochemical performance during ball milling of LFP precursor.

CHAPTER 2

SYNTHESIS OF LFP AND CHARACTERIZATION TECHNIQUES, AND ELECTRODE PREPRATION

2.1 INTRODUCTION

Through a solid-state ball milling reaction, we were able to synthesize olivine-structured $LiFePO_4$ (LFP) belongs to Pnma space group and has an orthorhombic structure, which is hexagonal packed structure of oxygen array where divalent Fe^{2+} ions occupy corner-shared octahedral structures shared by corners instead of an ongoing chain of edge-shared FeO_6 octahedral that might enhance electrical conductivity.. Whereas PO_4^{3-} are found in tetrahedral sites, chains of edge-shared octahedral sites are home to lithium ions [17], [18].

2.2 MATERIAL SYNTHESIS

Depending on its starting materials, $LiFePO_4$ exhibits a range of electrochemical capabilities. For the synthesis of $LiFePO_4$ stoichiometric amount of $LiOH.H_2O$ (Of Purity $\geqslant 99\%$), FeC_2O_4 (Of Purity $\geqslant 99\%$), and $N_2H_9PO_4$ (Of purity $\geqslant 99\%$) were used as precursors. To encounter the lithium loss at high temperature 10% access of lithium hydroxide was added. Starting precursors were mixed by a high energy ball mill in ethanol media. After mixing the powder was dried at 80 ℃ to remove the moisture because Iron oxalate is moisture gaining. Then the sample was calcined at 650 °C for 10 hours in slightly reductive environment to obtain $LiFePO_4$.

2.3 CHARACTERIZATION TECHNIQUES

2.3.1 X-RAY DIFFRACTION (XRD)

An effective method for locating crystalline phases in the sample material is X-ray diffraction (XRD). XRD is used to measure structural parameters like as strain, phase composition, grain size, and defect structure. X-ray beams strike the sample and are deflected by the atoms. The detector picks up the dispersed X-rays at an angle equal to the incident angle. Only when the crystal has been properly rotated does the peak appear on the diffractogram. In order to get positive peak interference on the diffractometer, Bragg's law must be met

$$2dsin\theta = n\lambda \qquad\qquad\qquad (9)$$

Where, n stands for order of diffraction, λ stands for wavelength of x-ray used, θ stands for the angle at which diffraction takes place called bragg's angle and d stands for inter planner distance [19].
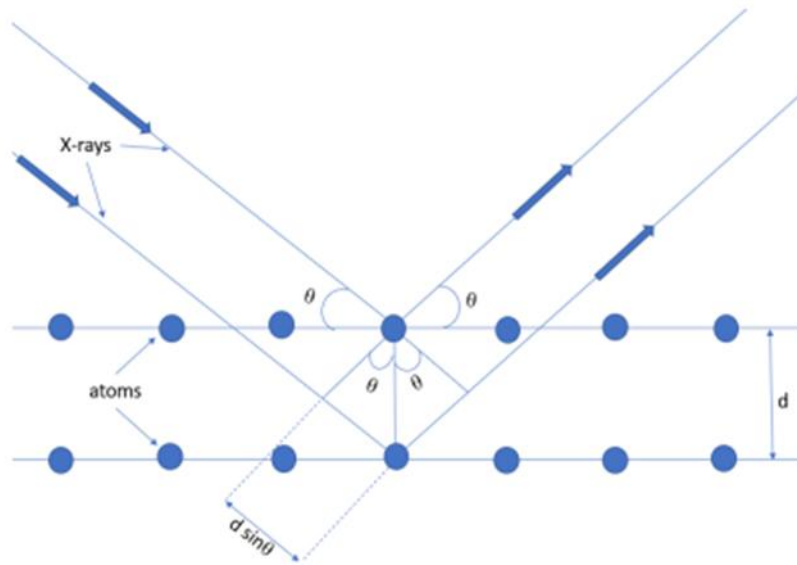

Fig 2.1: Schematic Diagram of Bragg's law

2.3.2 THERMAL GRAVIMETRIC ANALYSIS (TGA)

The relationship between weight change and temperature change is measured using TGA. The generated curve provides a variety of information, including a change in the sample's composition and the kinetics of a chemical reaction. TGA can provide a wide range of additional services, including:

1. Reaction speed and activation energy.

2. Moisture loss, absorption, and drying.

3. Calculate a sample's lifetime (related to thermal stability).

4. Oxidative organic material degradation in air/O2, metal oxidation in air, and thermal decomposition in an inert atmosphere.

5. The material's reaction to a reactive or corrosive environment.

When chemical bonds are broken, volatiles are lost with an increase in temperature, or weight loss happens in the sample due to desorption. While the sample's weight increase results from oxidation, absorption, or adsorption [20].

2.3.3 FTIR

Fourier change infrared (FTIR) spectroscopy is used to examine the vibrational properties of amino acids and cofactors, which are sensitive to tiny auxiliary changes. On the one hand, our strategy's requirement for specificity allows us to test in-depth the vibrational characteristics of almost all cofactors, amino corrosive side chains, and water particles. Instead, we'll use reaction-induced FTIR distinction spectroscopy to pick vibrations in comparison to certain chemical bunches that are present in a given response. Different methods are used to

differentiate between the IR markings of each accumulation of interested inside the arising reaction-induced FTIR distinction spectra [21].

2.4 ELECTRODE PREPARATION

Two electrode half coin-cells (CR2016) were built to see the electrochemical properties. In order to make the working electrodes, active material, Super P and PVDF was mixed in ratio of 70:10:10 dispersed in NMP solvent. This creates a homogeneous slurry, which was then deposited uniformly on an Al foil which acts as current collector using the "doctor blade" method. The solvent was then vaporized overnight at 120 °C in a vacuum oven. Next, 16mm-diameter round electrodes were cut, and they were weighed. For electrochemical testing of the synthesised LFP, the coin cells (CR2016) was fabricated using metallic lithium chip as the counter electrode with a separator called Celgard 2400 inside MBraun Lab Star glove box. A 1:1 (by volume) solution of 1 M $LiPF_6$ in DMC and EC was utilised as electrolyte.

CHAPTER 3

THERMAL, STRUCTURAL, CONDUCTIVITY AND ACTIVATION ENERGY ANALYSIS

3.1 THERMAL ANALYSIS

To choose the ideal calcination temperature and investigate the phase transition of the ball-milled raw material, DSC/TG analysis is necessary. Thermogravimetric analysis is used to calculate the change in the mass of the sample with temperature and to calculate the calcination temperature. The three-stage mass loss curve is shown by the TGA curve. The TGA curve mainly displays three stages of mass reduction. According to the diagram, the release of physically adsorbable water and the evaporation of organic molecules as gases constitute the first step of mass loss between 50 and 200 °C ($\Delta m=14\%$).
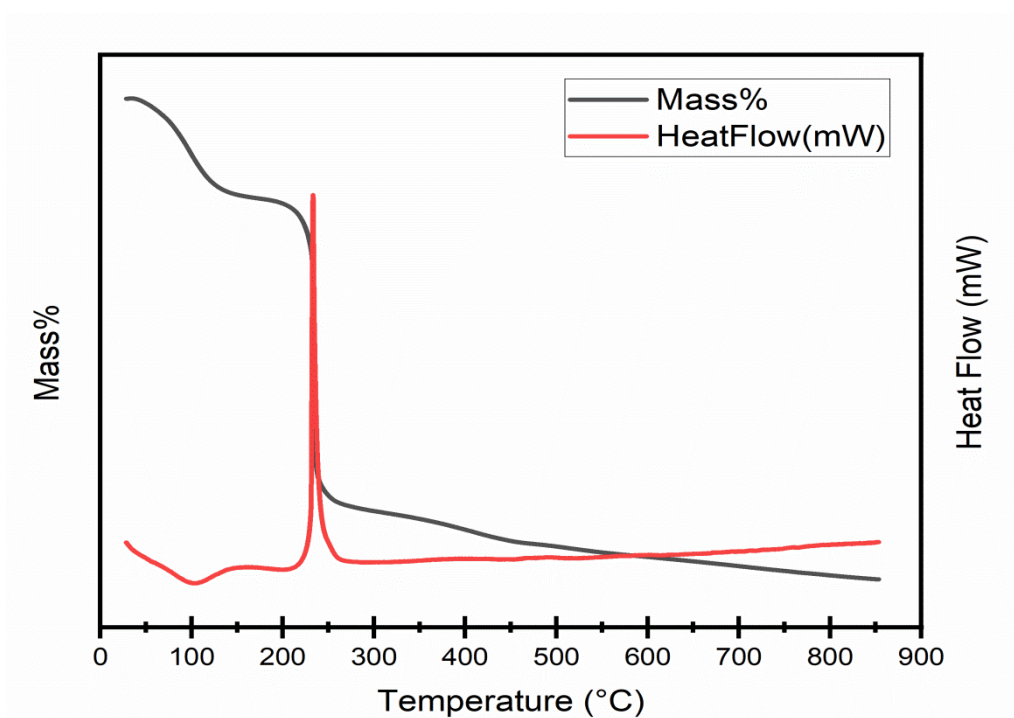

Fig 3.1: TGA and DSC curves of LFP under air atmosphere

Between 200 and 250 °C, there is a second stage of mass loss ($\Delta m = 38\%$), which corresponds to the thermal degradation of solvents such as alcohol. And in the final stage from 250 to 650, there is removal of elemental carbon and other gases such as NH_3, etc. Precursor mass becomes constant above 675 °C, indicating the onset of the olivine phase. Also there a large exothermic peak at 231°C between the temperature range of 200 – 300° C is also observed which represents that heat is released which represents the crystallization temperature means from this temperature crystallization of material starts. As a result, olivine $LiFePO_4$ phase production will occur between 675-700 °C. Nonetheless, the synthesized sample underwent a 10-hour phase and morphological optimization at 650 °C.

3.2 STRUCTURAL ANALYSIS

Figure 3.2 displays the pristine LFP sample observed XRD pattern. An orthorhombic system with a Pnma space group can be used to index all of the peaks in the resulting XRD pattern. There were no peaks for impurities such as $Li_3Fe_2(PO_4)_3$ and Fe_2O_3, which could have been brought on by iron oxidation during the procedure. The crystalline nature of the synthesized sample was shown by the sharp intense peaks. The average crystallite size found is 23 nm which is calculated using scherrer formula [22]

$$T = \frac{k\lambda}{\beta \cos\theta}$$
(10)

Where, T, λ, k θ , β are average crystallite size, wavelength of x-ray used, shape factor (k=0.9), angle at which diffraction takes place and FWHM respectively .
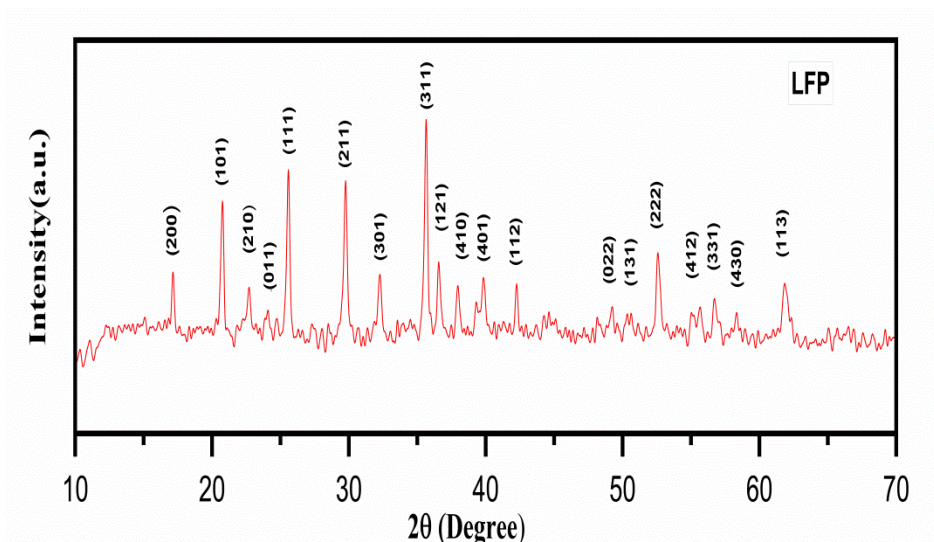
Fig.3.2: XRD pattern of synthesized pristine LFP

For the synthesized samples, Rietveld refinement was carried out to obtain quantitative structural data of the pristine LFP crystal lattice and it is found that the crystallographic parameters are: a $= 10.3072$ Å ; b $= 5.9969$ Å; c $= 4.6910$ Å with cell volume 289.9520 (Å)^3. The goodness of fitting is 1.09 which shows a good fit and best parameters. It is interesting that the LiFePO$_4$ sample's b-axis lattice parameter (6.001Å) is lower than the majority of published values. Moreover, the Rietveld refinement revealed that the lithium sites have no extra electron density (<0.2%), proving that the iron is entirely ordered. And the micro-strain was calculated using the W-H plot and is found to be 25×10^{-4}.
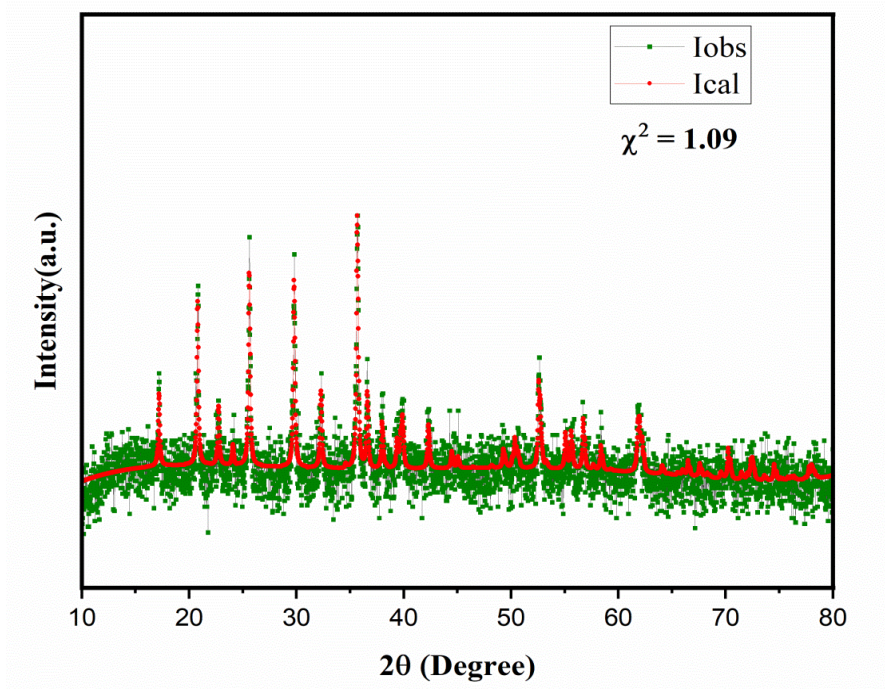
Fig.3.3: Rietveld refinement of pristine LFP

3.3 FTIR STUDY- CATION ENVIRONMENT

FTIR analysis of $LiFePO_4$ involves measuring the infrared spectrum of a powder sample in the range of 400-1250 cm^{-1}. In general, cation motion with regard to oxygen atoms is defined by in which manner they vibrate that are especially responsive to the cations point group regularity in the oxygen host matrix. As a result, FTIR spectroscopy can be used to investigate the cations' immediate surroundings in a crystal lattice of closely packed oxygen atoms. The local cationic arrangement of phospho-olivine is composed of LiO_6 and FeO_6 octahedra connected to PO_4^{-3} polyanions and can be described using factor group analysis and a molecular vibration model [13] . The peaks of the FTIR spectrum, located between 461 and 1136 cm^{-1}, are attributed to vibration of bending and stretching of the (PO_4^{-3}) ion. The basic vibrational frequencies of the (PO_4^{-3}) ions are 470, 632, 929, and 1034 cm-1.

Additionally, the bands in the 360–622 cm^{-1} spectral range are sensitive to the local lithium atmosphere. The broad band, as seen in Figure 3.4, provides evidence of polycrystalline nature and a decrease in phonon lifetime, demonstrating the absence of periodicity of lattice sites as a result of defects [23]. The characteristic ferrous ion absorption peak is at 636 cm^{-1} and is a part of the symmetric stretching vibration.
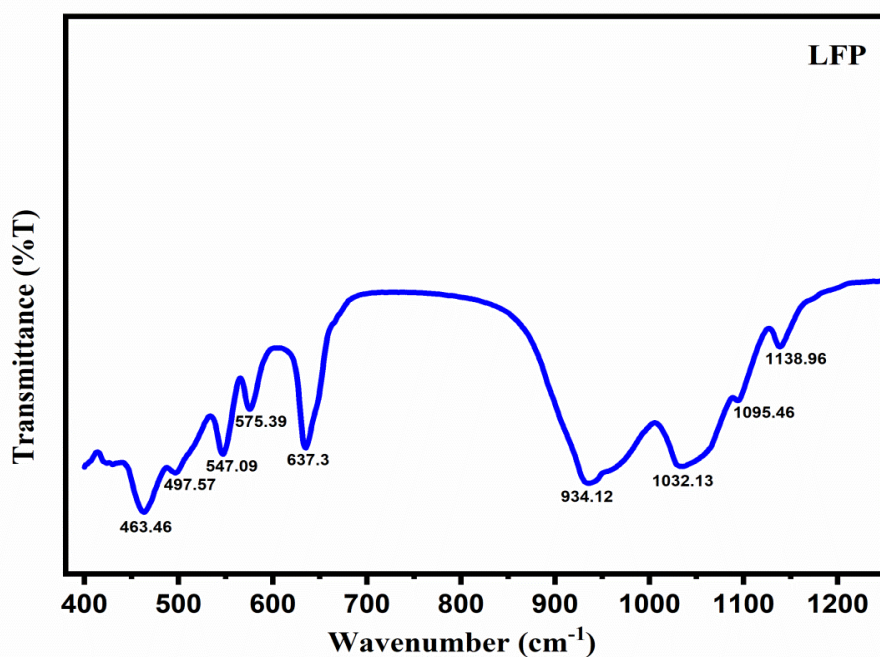

Fig.3.4: FTIR spectrum of synthesized pristine LFP sample in a range of 400-1250 cm^{-1}.

3.4 CONDUCTIVITY AND ACTIVATION ENERGY MEASUREMENTS

3.4.1 Pellet Formation and polishing: After the sintering process, the powder was brought to room temperature and ground for 30 minutes in a pestle and mortar. The obtained fine powder was compressed at a pressure of 60 MPa in a hydraulic press to create pellets with a diameter of 10 mm. To get rid of any remaining moisture, these pellets were subsequently dried for 30 minutes at 80°C temperature. Additionally, silver paste was used to polish both

of the pellets' surfaces in order to make them more conductive. The pellets were once again dried at 80°C temperature overnight after polishing.

3.4.2 D C Conductivity and activation energy

The figure 3.5 shows the variation of resistivity vs. temperature of synthesized pristine LFP sample and it shows exponential nature and the dc conductivity is calculated by [14]

$$\sigma = \frac{1}{\rho} \qquad (11)$$

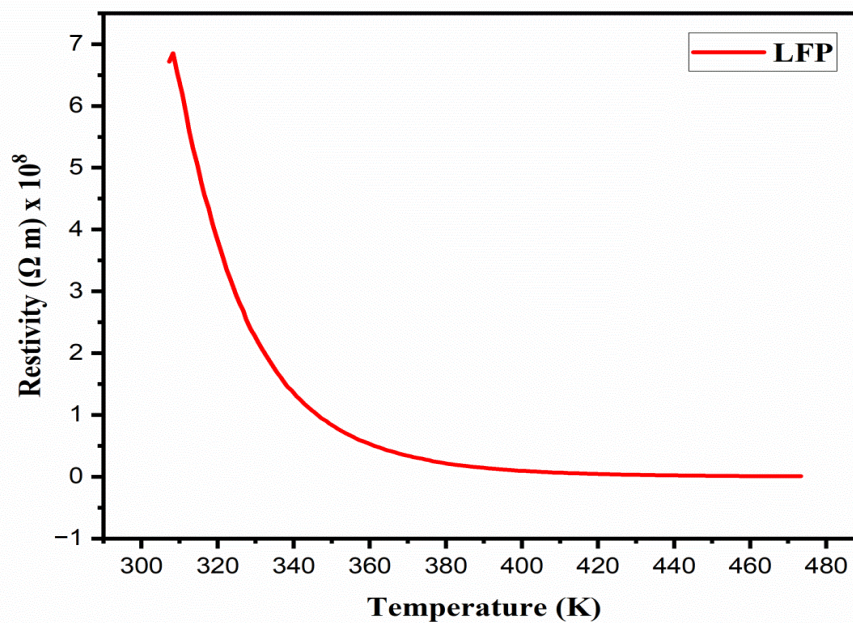Where, σ be the dc conductivity and ρ be the resistivity of the material.

Fig.3.5: Variation of resistivity with temperature.

A material's electrical conductivity is determined by how easily an electric current may pass through it. As we can see, increasing the temperature increases the dc conductivity of the material because increasing the temperature reduces the resistivity of the material, and the rise in the dc conductivity is almost exponential because the decrease in the resistivity is almost exponential and the pristine LFP has a conductivity of 10^{-9} S cm^{-1}, which is a fine matching with others and from these graphs it is clear that pristine LFP has insulating nature.

The link between activation energy and the reaction rate is quantitatively explained by the Arrhenius equation. The energy required for entering the transition state is referred to as the activation energy (E_a) in the Arrhenius equation. Along with the Arrhenius equation, the Eyring equation is also used to show a relationship between reaction rates and the transition for a one-step process given by [15]

$$k = \left(\frac{k_B T}{h}\right) \exp\left(-\frac{\Delta G}{RT}\right) \tag{12}$$

The Gibb's free energy of activation to reach the transition state is given by ΔG in the Eyring equation rather than additionally utilizing Ea. The Boltzmann and Planck constants, k_B and h, are indicated in the equation. Here the significant thing to remember is despite the equations seeming to be similar, it is demonstrated that the Gibbs free energy has both an entropic and an enthalpic component. This entropic component in the Arrhenius equation is represented by σ_0. The enthalpy and entropy of activation may also be used to represent the Gibbs free energy of activation as [24]

$$\Delta G = \Delta H - T \Delta S \tag{13}$$

Then, to estimate the approx relationships for a single molecule, one-step reaction hold [25]

$$E_a = \Delta H + RT \tag{14}$$

And [14], [15]

$$\sigma_0 = \left(\frac{KT}{h}\right) \exp\left(1 + \frac{\Delta S}{R}\right) \tag{15}$$

Though σ is temperature independent in the Arrhenius theory proper, there is a linear influence on T in this case. Ea, ΔG, and ΔH are frequently muddled and collectively referred to as the "activation energy" in sloppy language because of the comparatively modest size of $T\Delta S$ and RT at ordinary temperatures for the majority of reactions. However, the activation

energy has no bearing on the reaction's overall free energy change. Exergonic and endergonic reactions can occur in physical and chemical processes, although the spontaneity of a reaction has nothing to do with the activation energy. The activation energy has no effect on the total reaction energy change.

Activation energy is calculated using the Arrhenius plot and Arrhenius equation shown in fig.6 and it is found to be 0.59 eV. The minimal extra energy a reactive molecule requires to change into a product is referred to as activation energy. [22]

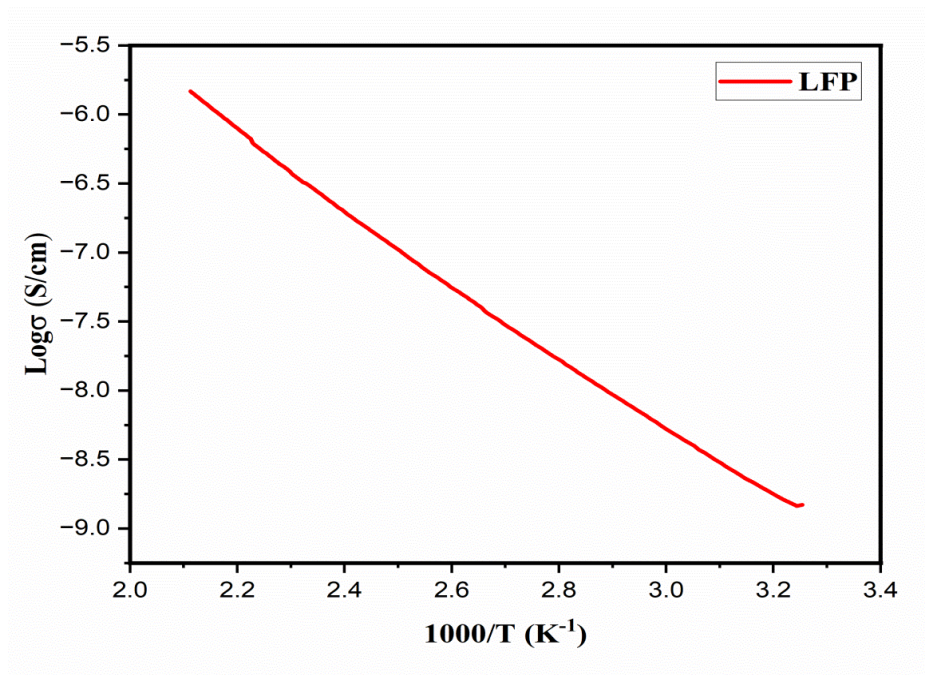$$\sigma_{dc} = \sigma_0 \exp(-E_a / KT) \tag{16}$$

Fig.3.6: Arrhenius plot, variation of conductivity with temperature for as-synthesized LFP

Here symbols K, T, E_a, σ_0, σ_{dc} represents constant, Temperature, Activation energy, electrical conductivity at temperature tends to infinite, electrical conductivity at a temperature T.

CHAPTER 4

ELECTROCHEMICAL CHARACTERIZATION

4.1 CYCLIC VOLTAMMETRY ANALYSIS

 Cyclic voltammetry curves of pristine LFP are displayed in the figure 4.1. As demonstrated in Figure, it only display the distinctive redox peaks of pristine LFP in the potential range of 2.8-4.2 V. The flow of ions increases during charging as potential rises, peaking at a potential of 3.7V, before decreasing and becoming zero, indicating that the cell is fully charged. This tendency also occurs while the cell is being discharged. The separation potential between the anodic and cathodic peak on the cyclic voltammogram is a significant parameter to assess the reversibility of the electrochemical process. When Fe^{3+} ($FePO_4$) and Fe^{2+} ($LiFePO_4$) undergo two-phase transition reactions as oxidation and reduction, respectively, CV curves have peaks at about 3.6 and 3.3 V. On the Y axis, the reduction peak is in the positive direction, whereas the oxidation peak is in the opposite direction. The host lattice's internal electrode response is more reversible because the fastest lithium ion transport during the first cycle is represented by the highest redox intensity. After the first cycle, the peaks grow ever-narrower and less intense, indicating a decline in activity and kinetics.
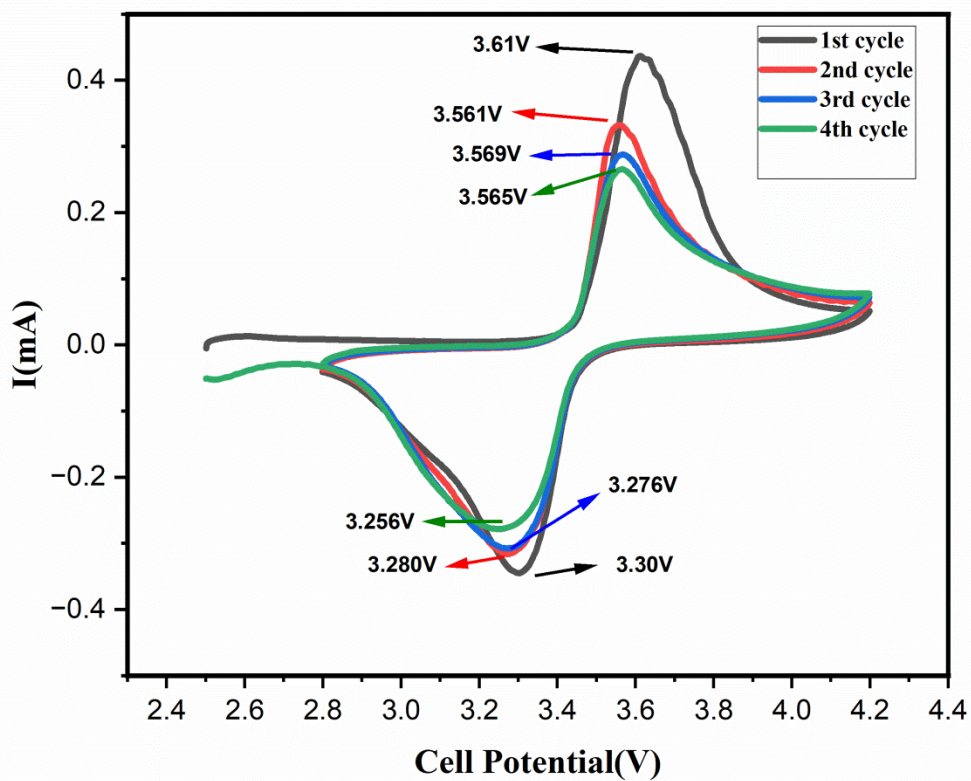
Fig.4.1: Cyclic voltammograms (CV) of 1st 4cycles of pristine LFP at a scan rate of 0.05mV/s

The table 2 below compares the equivalent ratios of the current intensities of anode and cathode. For the lithium redox process to be reversible, the I_A/I_C ratio needs to be close to 1.

Table 4.1. CV results of pristine LFP sample

Cycle	I_A (mA)	I_C (mA)	I_A/I_C
1st	0.43	0.34	1.26
2nd	0.33	0.31	1.06
3rd	0.28	0.30	0.93
4th	0.26	0.27	0.96

4.2 EIS ANALYSIS

To examine the cell impedance, the EIS of cells was carried out. The fabricated electrode materials are examined using EIS measurement since a cell's internal impedance is an important factor that directly affects how well it performs electrochemically. Figure 4.2 below displays the EIS spectra of the LFP sample scanned in frequency varying from 10 mHz to 100 kHz at a voltage of 5 mVAs can be observed, the curve has two areas that correspond to the low-frequency and high-frequency domains, respectively, a straight line and a semicircle. The resistance between the electrode and electrolyte, or the cell's ohmic resistance (Rs), is typically displayed as an intercept along the Z′ axis in the high-frequency domain. [15]. The electrochemical reactions that occur at the electrode/electrolyte interface are mostly responsible for the semicircle in the middle frequency band that displays charge-transfer resistanc (Rct). The slanted line represents Warburg impedance (Zw), which represents the net movement of Li-ion in the electrode active material in the low-frequency zone [15]. The equation given below determines the value of lithium-ion diffusion coefficient in bulk electrode materials [14]

$$D = \frac{R^2 T^2}{2A^2 n^4 F^4 C^2 \sigma W^2} \tag{17}$$

where n represents how many electrons are involved in the reaction process (1 in this case), D be the diffusion coefficient for Li^+ ions(cm^2 s^{-1}), F is the Faraday constant (96 486 C/mol), T be the absolute temperature in units of Kelvin (K), R be the gas constant (8.314 J/mol K), A be the area of electrode (cm^2), C represents the amount of lithium ions i.e. concentration (7.69 103 mol cm^3), and $\sigma^2{}_w$ is the Warburg factor, which is connected to Z' by [26]

$$Z' = R_s + R_{ct} + \sigma_w \, \omega^{-0.5} \tag{18}$$

And the lithium-ion diffusion coefficient found to be is $3.9 \times 10^{-14} cm^2$ s^{-1} and σ_w is found to be 76.91 Ω $s^{-0.5}$.
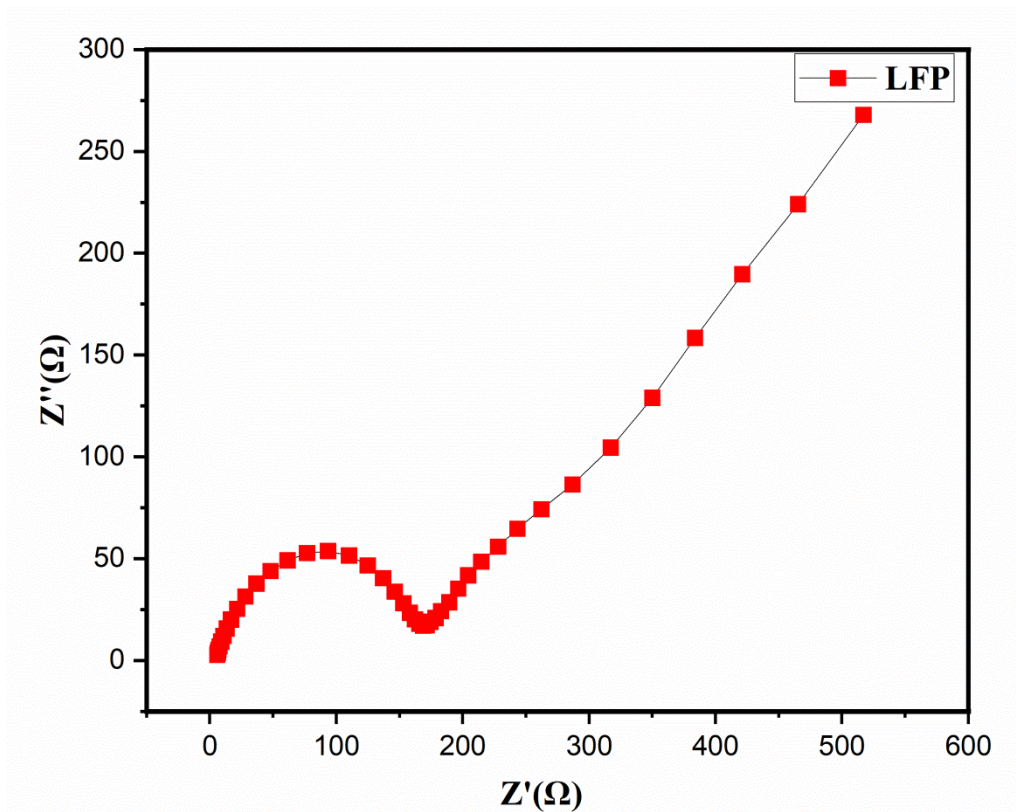
Fig.4.2: Impedance spectra of synthesized pristine LFP sample

4.3 GCD ANALYSIS

Fig.4.3 below shows the GCD of the first 3 cycles of synthesized Pristine LFP at 0.5C in the range of 2.5-4.2V. From these 3 cycles we can find that the 1st cycle of pristine LFP has a specific discharge capacity of 52(±5) mAh/g. LiFePO$_4$ particles with better crystallinity, smaller sizes, and lower impurity levels often exhibit larger discharge capacities. A wide flat Charge/discharge plateaus between 3.6 V and 3.3 V were present on all of the charge/discharge curves. As we can see from GCD curve the charge/discharge voltage plateau results in a very approving accord with the CV profile. From the graph it is clear that the 1st cycle shows less polarisation potential hence, lithium-ion diffusion is more which later on cycles will decrease. The table below shows the potential difference during the first three cycles between the charge and discharge plateaus.

Table 4.2. GCD performance of synthesized pristine LFP

cycle	Charge plateau Voltage(V)	Discharge plateau Voltage(V)	ΔV
1st	3.58	3.32	0.26
2nd	3.55	3.31	0.23
3rd	3.58	3.30	0.28

The polarization of the cell system was associated with the voltage (ΔV) differential between the flat charge and discharge plateaus
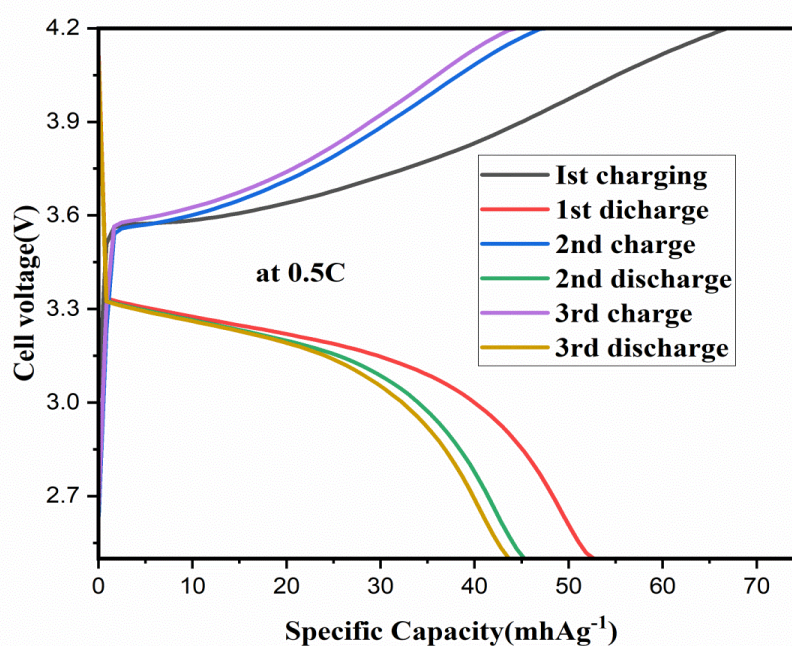

Fig.4.3: First 3 cycles of charge/discharge curves of pristine LFP at 0.5C rate

4.4 CYCLING PERFORMANCE

Up to 50 cycles at 0.5 charge-discharge rates were used to test the cycle performance of cells containing pristine LiFePO$_4$, and the results are shown in Fig.10. below. An outstanding long-

term cycling property is displayed by the cells. There is a slight capacity loss in the cells, after some time the capacity loss becomes constant followed by a prominent capacity retention. This is because it has the lowest polarisation potential, which facilitates quick mobility of lithium ions and electrochemical kinetic
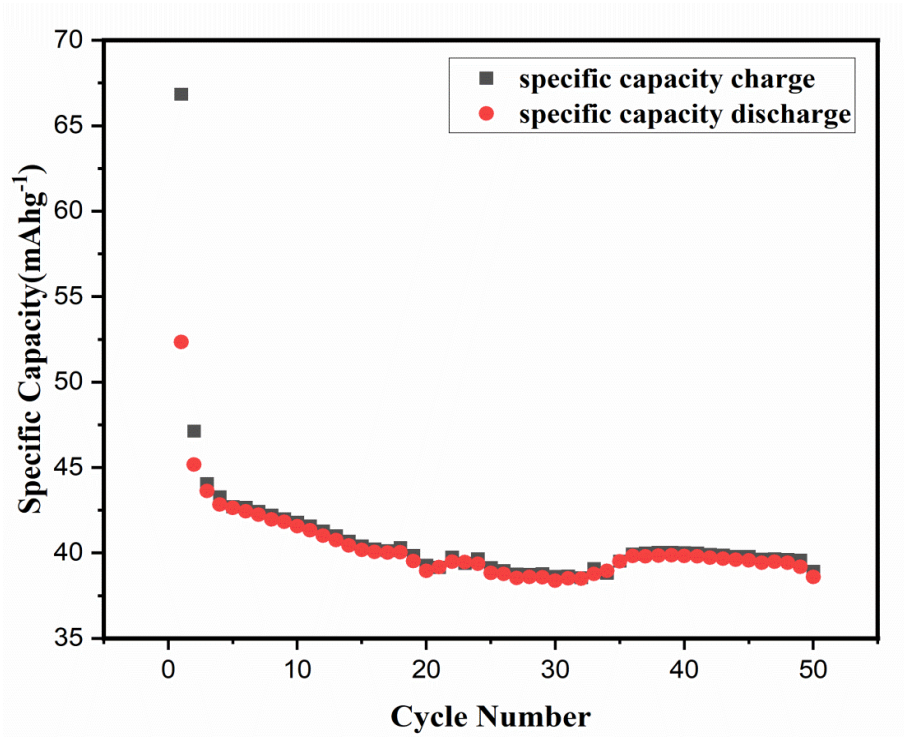

Fig.4.4: Cycling performance of synthesized pristine LFP at 0.5C

4.3 COULOMBIC EFFICIENCY

Fig.11. shows the coulombic efficiency of pristine LFP with cycle number and it shows a coulombic efficiency of 99% after 50 cycles. Efficiency that is lower than 100% indicates that numerous active lithium ions were intercalated into or deposited on the anode and cannot return to the cathode, potentially leading to a quick capacity fall down. Coulombic efficiency is defined as the capacity ratio between discharge and charge.
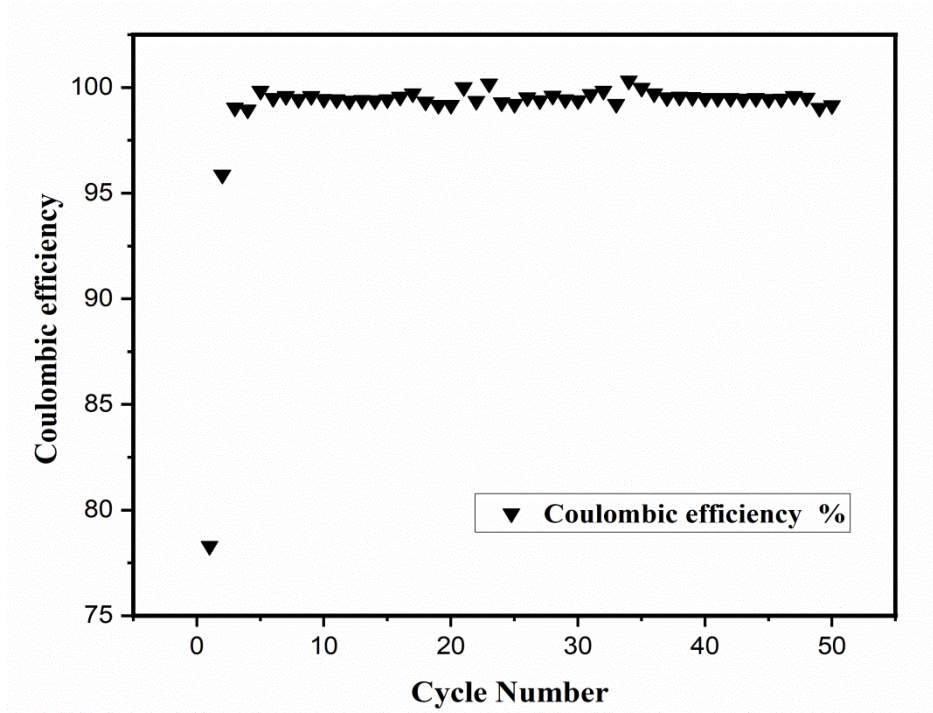
Fig.4.5: Coulombic efficiency of Pristine LFP

The Coulombic efficiency is frequently used to define the released battery capacity. It describes the ratio between the capacity for charging during the same cycle and the capacity for discharging after a complete charge. Typically, it is only a little bit less than 1. Coulombic efficiency is given by [27]

$$\text{Coulombic efficiency} = \frac{\text{Discharge Capacity}}{\text{Charge Capacity}} \times 100 \qquad (19)$$

Here we can see that pristine LFP cell has a Coulombic efficiency of greater than 99%. An efficiency of less than 100% shown that a large number of active lithium ions were intercalated into or deposited on the anode and were unable to return to the cathode.

CHAPTER 5

CONCLUSION

Here in this study, pristine LFP sample were successfully synthesized using the process of solid-state reaction route. TGA/DSC curve shows the mass loss of the sample with temperature in different phases and shows the phase formation of LFP at 650 $^\circ$C and also shows that the material crystallizes at 230 ºC but the stable orthorhombic phase of LFP is formed at 650 ºC. The crystallite size and micro-strain was calculated using scherrer formula and W-H plot and comes out to be 23 nm and 25×10^{-4} respectively. And there was no evidence of any impurity in the synthesized material such as $Li_3Fe_2(PO_4)_3$ or Fe_2O_3. FTIR reveal the existence of vibrational modes corresponding to $(PO_4)^{3-}$ tetrahedral structures and shows the vibration and stretching of $(PO_4)^{3-}$ in different environment. Conductivity measurement shows that pristine LFP shows an insulating nature with dc conductivity in the range of 10^{-9} S/cm with activation energy 0.59 eV calculated using Arrhenius equation. CV analysis only shows the redox peaks of LFP at 3.6 V and 3.3 V. EIS analysis shows the charge transfer resistance of the cell is 170 Ohm. GCD shows that 1st cycle of pristine LFP shows a discharge capacity of 52($\pm$5)mAh/g at 0.5C.

REFERENCES:

[1]   "Lithium-ion battery."

[2]   "History_of_the_lithium-ion_battery".

[3]   B. Wu *et al.*, "Morphology controllable synthesis and electrochemical performance of LiCoO2 for lithium-ion batteries," *Electrochim Acta*, vol. 209, pp. 315–322, Aug. 2016, doi: 10.1016/j.electacta.2016.05.085.

[4]   S. H. Choi, J. Kim, and Y. S. Yoon, "Self-discharge analysis of licoo2 for lithium batteries," *J Power Sources*, vol. 138, no. 1–2, pp. 283–287, Nov. 2004, doi: 10.1016/j.jpowsour.2004.06.047.

[5]   T. Utsunomiya, O. Hatozaki, N. Yoshimoto, M. Egashira, and M. Morita, "Self-discharge behavior and its temperature dependence of carbon electrodes in lithium-ion batteries," *J Power Sources*, vol. 196, no. 20, pp. 8598–8603, Oct. 2011, doi: 10.1016/j.jpowsour.2011.05.066.

[6]   R. Yazami and Y. Ozawa, "A kinetics study of self-discharge of spinel electrodes in Li/Li xMn2O4 cells," in *Journal of Power Sources*, Feb. 2006, pp. 251–257. doi: 10.1016/j.jpowsour.2005.10.012.

[7]   J. P. Schmidt, A. Weber, and E. Ivers-Tiffée, "A novel and fast method of characterizing the self-discharge behavior of lithium-ion cells using a pulse-measurement technique," *J Power Sources*, vol. 274, pp. 1231–1238, Jan. 2015, doi: 10.1016/j.jpowsour.2014.10.163.

[8]   Y. Zhang, P. Xin, and Q. Yao, "Electrochemical performance of LiFePO4/C synthesized by sol-gel method as cathode for aqueous lithium ion batteries," *J Alloys Compd*, vol. 741, pp. 404–408, Apr. 2018, doi: 10.1016/j.jallcom.2018.01.083.

[9]   K. Konstantinov *et al.*, "New approach for synthesis of carbon-mixed LiFePO4 cathode materials," in *Electrochimica Acta*, Nov. 2004, pp. 421–426. doi: 10.1016/j.electacta.2004.05.049.

[10]   S. L. Bewlay, K. Konstantinov, G. X. Wang, S. X. Dou, and H. K. Liu, "Conductivity improvements to spray-produced LiFePO4 by addition of a carbon source," *Mater Lett*, vol. 58, no. 11, pp. 1788–1791, Apr. 2004, doi: 10.1016/j.matlet.2003.11.008.

[11]   B. M. Kerbel, L. M. Katsnelson, and Y. V. Falkovich, "Continuous solid-phase synthesis of nanostructured lithium iron phosphate powders in air," *Ceram Int*, vol. 44, no. 7, pp. 8397–8402, May 2018, doi: 10.1016/j.ceramint.2018.02.032.

[12]   Y. Zhang, P. Xin, and Q. Yao, "Electrochemical performance of LiFePO4/C synthesized by sol-gel method as cathode for aqueous lithium ion batteries," *J Alloys Compd*, vol. 741, pp. 404–408, Apr. 2018, doi: 10.1016/j.jallcom.2018.01.083.

[13]   Z. Zhang, M. Wang, J. Xu, F. Shi, M. Li, and Y. Gao, "Modification of Lithium Iron Phosphate by Carbon Coating," *Int J Electrochem Sci*, vol. 14, no. 11, pp. 10622–10632, 2019, doi: 10.20964/2019.11.22.

[14]   R. Saroha, A. K. Panwar, Y. Sharma, P. K. Tyagi, and S. Ghosh, "Development of surface functionalized ZnO-doped LiFePO 4 /C composites as alternative cathode material for lithium

ion batteries," *Appl Surf Sci*, vol. 394, pp. 25–36, Feb. 2017, doi: 10.1016/j.apsusc.2016.09.105.

[15]   R. Saroha and A. K. Panwar, "Effect of in situ pyrolysis of acetylene (C2H2) gas as a carbon source on the electrochemical performance of LiFePO4 for rechargeable lithium-ion batteries," *J Phys D Appl Phys*, vol. 50, no. 25, May 2017, doi: 10.1088/1361-6463/aa708c.

[16]   J. Lee, P. Kumar, G. Lee, B. M. Moudgil, and R. K. Singh, "Electrochemical performance of surfactant-processed LiFePO4 as a cathode material for lithium-ion rechargeable batteries," *Ionics (Kiel)*, vol. 19, no. 2, pp. 371–378, Feb. 2013, doi: 10.1007/s11581-012-0830-9.

[17]   M. Morcrette, C. Wurm, and C. Masquelier, "On the way to the optimization of Li 3 Fe 2 (PO 4) 3 positive electrode materials," 2002. [Online]. Available: www.elsevier.com/locate/ssscie

[18]   S. H. Luo, Z. L. Tang, J. B. Lu, J. R. Li, and Z. T. Zhang, "Improvement of the Electrochemical Performance of LiFePO$_4$ Cathode Composite Material Using a In Situ Pyrolysis Carbon Synthesis Procedure," *Key Eng Mater*, vol. 336–338, pp. 466–469, Apr. 2007, doi: 10.4028/www.scientific.net/kem.336-338.466.

[19]   Y. Li *et al.*, "Synthesis of graphene-supported LiFePO4/C materials via solid-state method using LiFePO4(OH) as precursors," *Journal of Solid State Electrochemistry*, vol. 26, no. 11, pp. 2595–2600, Nov. 2022, doi: 10.1007/s10008-022-05266-z.

[20]   J. Im, K. Heo, S.-W. Kang, H. Jeong, J. Kim, and J. Lim, " LiFePO 4 Synthesis using Refined Li 3 PO 4 from Wastewater in Li-Ion Battery Recycling Process ," *J Electrochem Soc*, vol. 166, no. 15, pp. A3861–A3868, 2019, doi: 10.1149/2.1331915jes.

[21]   Y. Kuk, J. Hwang, D. Nam, and J. Kim, "Facile synthesis of high-performance LiFePO4-reduced graphene oxide composites using ball milling," *Ionics (Kiel)*, vol. 26, no. 6, pp. 2803–2812, Jun. 2020, doi: 10.1007/s11581-019-03395-6.

[22]   W. J. Zhang, "Structure and performance of LiFePO4 cathode materials: A review," *Journal of Power Sources*, vol. 196, no. 6. pp. 2962–2970, Mar. 15, 2011. doi: 10.1016/j.jpowsour.2010.11.113.

[23]   A. Ait Salah *et al.*, "FTIR features of lithium-iron phosphates as electrode materials for rechargeable lithium batteries," *Spectrochim Acta A Mol Biomol Spectrosc*, vol. 65, no. 5, pp. 1007–1013, Dec. 2006, doi: 10.1016/j.saa.2006.01.019.

[24]   "Gibbs_free_energy".

[25]   "Activation energy."

[26]   S. B. Lee, I. C. Jang, H. H. Lim, V. Aravindan, H. S. Kim, and Y. S. Lee, "Preparation and electrochemical characterization of LiFePO$_4$ nanoparticles with high rate capability by a sol-gel method," *J Alloys Compd*, vol. 491, no. 1–2, pp. 668–672, Feb. 2010, doi: 10.1016/j.jallcom.2009.11.037.

[27]   I. Stenina, P. Minakova, T. Kulova, and A. Yaroslavtsev, "Electrochemical Properties of LiFePO$_4$ Cathodes: The Effect of Carbon Additives," *Batteries*, vol. 8, no. 9, Sep. 2022, doi: 10.3390/batteries8090111.

APPENDIX

42

43

CERTIFICATE

Department of Physics
Netaji Subhas University of Technology
Sec-3, Dwarka, New Delhi-110078, India

Certificate of Presentation

This certificate is proudly awarded to Prof./Dr./Mr./Ms. *Manish Kumar*
from *DTU, New Delhi*
Paper Title: *Structural, Physicochemical - - - - - - - - -- Ball Milling*
For your excellent oral/ poster presentation at the conference and your significant contribution to the success of **International Conference on Advanced Materials for Emerging Technologies (ICAMET- 2023)**, held during **May 4-6, 2023**, at Netaji Subhas University of Technology, New Delhi - 110078, India.

Dr. Anurag Gaur
Convener

ICAMET
May 4-6, 2023

Prof. Ranjana Jha
Conference Chair

PAYMENT DETAILS

INTERNATIONAL CONFERENCE ON
ADVANCED MATERIALS FOR EMERGING TECHNOLOGIES
May 4-6, 2023
Department of Physics
Netaji Subhas University of Technology (NSUT)
Sec-3, Dwarka, New Delhi-110078, India

No. **066**

RECEIPT

Date 04.05.2023

Received with thanks from Prof./Dr./Mr./Ms. Manish ....

....

a Sum of Rupees (in words) Two thousand only ——

on account of Registration/Accommodation/Miscellaneous ....

.... by online Transfer transaction ID No. T23042412255700 Dated ....
— 53081584

ICAMET
May 4-6, 2023

Convener

₹ 2000/=

ACCEPTANCE REPORT

DTU.
Delhi Technological
UNIVERSITY

Amrish kumar panwar <amrish.phy@dtu.ac.in>

regarding your paper presented in ICAMET 2023
1 message

International Conference <icamet@nsut.ac.in>   Tue, May 30, 2023 at 1:23 PM
To: amrish.phy@dtu.ac.in

Dear Prof. Panwar, Greetings!

Your paper entitled "Structural, morphological, electrical, and electrochemical performance of $LiFePO_4$ synthesized using ball milling" presented by Manish Kumar et al in ICAMET 2023 has been accepted after the internal review process for publication in the Conference proceedings published by Royal Book Publishing-Eleyon Publishers, Tamil Nādu, India. The formatting and other details in this regard will be communicated later.

Thank you for presenting your work in ICAMET-2023.

Organising Committee
ICAMET-2023